




Article

# Permanent Magnet Installation Optimization of Outer Rotor PMSM Depending on Adding Auxiliary Teeth

Jiayin Su, Rui Nie \*, Peixin Wang, Shuai Xu, Jing Liang  and Jikai Si

School of Electrical and Information Engineering, Zhengzhou University, Zhengzhou 450001, China; sujiayin1122@163.com (J.S.); wangpeixin509@126.com (P.W.); xszzu2020@zzu.edu.cn (S.X.); liangjing@zzu.edu.cn (J.L.); sijikai@zzu.edu.cn (J.S.)

\* Correspondence: nierui@zzu.edu.cn

**Abstract:** To reduce the influence of the permanent magnet (PM) installation error on the electromagnetic characteristics of the outer rotor permanent magnet synchronous motor (OPMSM), the rotor structure of the OPMSM is optimized in this paper. The optimization method of adding auxiliary teeth on the surface of the rotor core is studied, and the influence of different auxiliary teeth heights on the electromagnetic performance of OPMSM is analyzed. It is found that adding auxiliary teeth with suitable height can greatly reduce the installation error of the PM, increase the mechanical stability of the motor, and ensure that the electromagnetic characteristics of the motor remain at a good level. Firstly, the topology and parameters of the motor proposed in this paper are introduced and analyzed. Secondly, the influence of PM installation error on the electromagnetic performance of the motor is analyzed based on the finite element method (FEM), and the necessity of eliminating PM installation error is demonstrated. Then, the parametric scanning method is used to analyze the influence of auxiliary teeth height change on the electromagnetic performance of the motor, and the selection standard of the optimal auxiliary teeth height is determined. By comparing and analyzing OPMSM with different sizes and different pole–slot ratios, the universality of the conclusions is demonstrated.

**Keywords:** outer rotor PMSM; electromagnetic characteristic; permanent magnet installation; permanent magnet tolerances; parametric scanning method



**Citation:** Su, J.; Nie, R.; Wang, P.; Xu, S.; Liang, J.; Si, J. Permanent Magnet Installation Optimization of Outer Rotor PMSM Depending on Adding Auxiliary Teeth. *World Electr. Veh. J.* **2024**, *15*, 271. <https://doi.org/10.3390/wevj15060271>

Academic Editor: Joeri Van Mierlo

Received: 16 May 2024

Revised: 11 June 2024

Accepted: 17 June 2024

Published: 19 June 2024



**Copyright:** © 2024 by the authors. Licensee MDPI, Basel, Switzerland. This article is an open access article distributed under the terms and conditions of the Creative Commons Attribution (CC BY) license (<https://creativecommons.org/licenses/by/4.0/>).

## 1. Introduction

Permanent magnet synchronous motor (PMSM), due to its high torque density, high power factors, and small torque ripple [1–3], has gradually replaced brushed DC motors and AC induction motors, widely used in military and industrial fields, especially in electric automobile and robots [4–6]. The outer rotor structure is mostly used in low-speed and high-torque working environments because of its higher torque density, smaller torque ripple, and more stable structure [7]. Outer rotor PMSM (OPMSM) mostly adopts fractional slot concentrated winding, compared with integral slot winding, the slot fill factor of fractional slot concentrated winding is greatly improved, the extension length of the winding end is greatly shortened, the amount of copper is reduced, and the cost is saved. It is conducive to miniaturization and lightweight of the motor, saving production hours, and realizing production automation [8–10]. The rotor of OPMSM usually adopts the surface-mounted structure, which is the PM directly mounted on the surface of the rotor core. This structure leads to low installation accuracy and large installation errors of PM. The installation error of PM has an impact on some electromagnetic properties of the motor, such as torque, torque ripple, and cogging torque, limiting the performance of the OPMSM.

To reduce the influence of PM installation errors on motor performance, many methods are proposed. In [11], an outer rotor interior PMSM (IPMSM) is proposed, which almost eliminates the PM installation error. This paper also slots on the rotor core to optimize

the flux path reluctance, which plays a role in reducing the cogging torque. However, the PM embedding process of interior PM structure is complicated and the assembly cost is high. The authors in [12–14] study the influence of manufacturing tolerances on motor performance during motor production. In [12], the influence of manufacturing tolerance on the cogging torque of PMSM is analyzed by combining experiment and theory, it is concluded that the stator inner diameter tolerance has the greatest influence on the cogging torque, followed by the PM tolerance. It is proposed that special design and optimization of key tolerances must be carried out in large-scale production of motors, and a manufacturing method for producing stator and rotor stacks is proposed in this paper, which can reduce the cogging torque caused by error by about 50%. However, only the stator and rotor are analyzed and optimized, and the optimization method of PM is not mentioned. The influence of PM shape error on the electromagnetic characteristics of the motor is studied and the relationship between the width and thickness of the PM and the cogging torque characteristics of the motor is analyzed in [15,16], but the influence of the installation position error of the PM is not considered. The influence of PM installation position on cogging torque is studied in [17,18]. In [17], the parameter expression of PM installation position and cogging torque is derived by energy method and flux path analysis. In [18], the expected distribution of PM installation accuracy and cogging torque is calculated by statistical method, and a method of PM installation accuracy required to achieve the expected cogging torque is provided for reference, but the specific method of improving PM installation is not mentioned in [18].

In summary, the installation error of PM has a great influence on the electromagnetic characteristics of the motor, but there is still a lack of research on the specific methods to improve the installation accuracy of PM. In this paper, the optimization method of adding auxiliary teeth to the rotor core is studied, which can facilitate the installation of PM and increase PM installation accuracy. The optimized motor is similar to the surface-mounted OPMSM in topology, but its electromagnetic characteristics are close to the surface-mounted OPMSM, it combines the advantages of the two structures. The optimized motor has mechanical stability, the characteristics of convenient PM installation of the surface-embedded structure, and the good electromagnetic characteristics of the surface-mounted structure. The influence of different auxiliary teeth heights on the electromagnetic performance of OPMSM is analyzed, the selection standard of the optimal auxiliary teeth height is determined, and the general applicability of the conclusion is verified. It can provide a design direction for such motor designers to improve the PM installation accuracy and take the electromagnetic performance into account.

In this paper, a 30-pole and 27-slot OPMSM is used as an example for modeling and analysis. The rest of this paper is organized as follows: the topological structure of the proposed motor is introduced in Section 2. In Section 3, the influence of PM installation error on the electromagnetic performance of OPMSM is analyzed, and the necessity of eliminating the PM installation error is demonstrated. In Section 4, the parametric scanning method is used to analyze the optimization method of adding auxiliary teeth to the rotor core, and the selection standard of the best auxiliary teeth height is determined, the OPMSM with different sizes and pole–slot ratios is compared and analyzed to verify the universality of the conclusion. Finally, Section 5 summarizes some conclusions.

## 2. Topology Structure and Parameters of the Proposed Motor

The OPMSM topology structure studied in this paper is shown in Figure 1. The motor is mainly composed of rotor, stator, PMs, and winding.

When the inner rotor motor is running at a high speed, the PM is subjected to a huge centrifugal force. How to avoid the displacement and shedding of the PM during rotation is an important issue that must be paid attention to in the design of the inner rotor motor. The common method is to use a better binder or to add a non-magnetic sheath on the outside of the rotor to ensure the safety of the PM, which increases the production cost of the motor, but the outer rotor structure does not need to consider these problems, because

the centrifugal force generated during the rotation of the motor rotor will make the PM more fit the rotor surface, and the outer rotor motor is generally not used for high-speed rotation environment. In addition, the motor with the outer rotor substructure has a larger air gap diameter, according to (1), the electromagnetic torque of the outer rotor motor is larger than that of the inner rotor motor of the same scale. The structural characteristics of OPMSM determine the large number of PM in the rotor part, which is one of the main reasons why the PM of OPMSM is difficult to install.

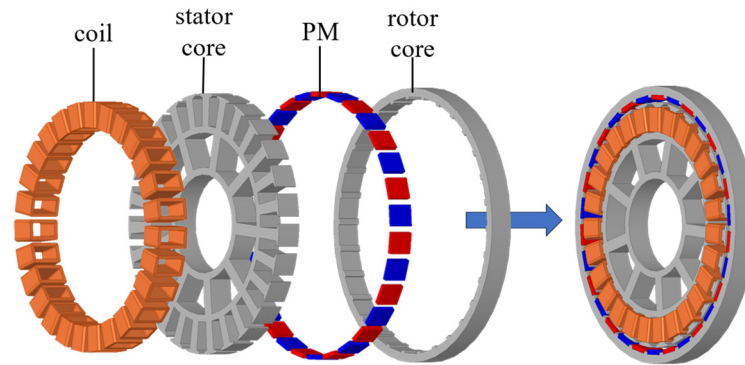


**Figure 1.** The structure of OPMSM proposed in this paper.

$$T \propto D_{air}^2 \quad (1)$$

By adding auxiliary teeth on the surface of the rotor core, the installation accuracy of the PM can be greatly improved, and the adverse effects of the PM installation error on the motor can be reduced. The optimized structure is shown in Figure 2.

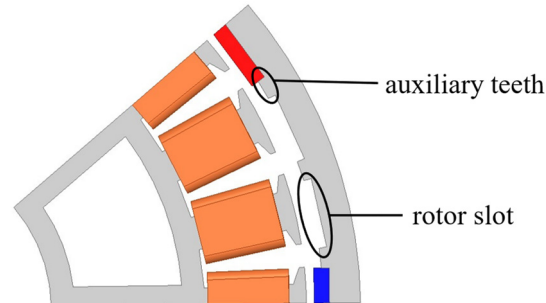


**Figure 2.** The structure of motor rotor with auxiliary teeth.

Different from the general surface-embedded structure, the rotor teeth height of this motor is small, and its magnetic circuit characteristics are closer to the surface-mounted PMSM (SPMSM): the reluctance of the d-axis and q-axis is approximately the same, so the electromagnetic characteristics of the optimized motor are also closer to the SPMSM. Compared with the SPMSM, it has better mechanical stability, convenient installation of PMs, and high installation accuracy; compared with the surface-embedded PMSM (SEPMSM), it has lower cost, better magnetic circuit characteristics, lower requirements for rotor machining accuracy, and higher machining fault tolerance. The specific structural parameters of the OPMSM proposed in this paper are shown in Table 1.

**Table 1.** The parameters of OPMSM studied in this paper.

Parameters	Values
Stator inner diameter	40 mm
Stator outer diameter	106 mm
Number of phases	3
Number of stator slot	27

Table 1. Cont.

Parameters	Values
Number of rotor pole	30
Rotor inner diameter (without tooth)	114 mm
Rotor outer diameter	120 mm
Thickness of PM	2 mm
Width of PM	9 mm
Stator teeth height	1 mm
Number of winding coils	30

### 3. Influence Analysis of PM Installation Error

In this section, the FEM is used to compare and analyze the electromagnetic characteristics and magnetic field distortion of the motor under the error of PM installation and the ideal installation state, which shows the influence of PM installation error on the electromagnetic performance of the motor. The necessity of eliminating the installation error of PM is demonstrated.

All the S-pole PMs of the OPMSM are counterclockwise shifted by 1 mechanical angle to indicate the possible error of PM installation as shown in Figure 3. It is difficult to judge such a difference in human vision.

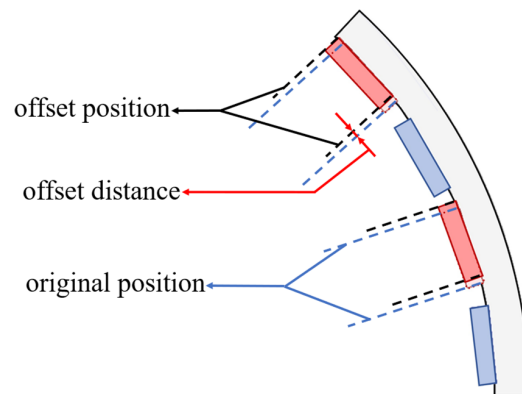


Figure 3. PM offset of OPMSM.

#### 3.1. Cogging Torque

Cogging torque is a unique electromagnetic characteristic of PM motor, when the rotor of the PM motor rotates, the cogging torque is an additional pulsating torque, which does not increase or decrease the average effective torque of the motor, but it causes speed fluctuation, vibration, and noise of the motor, especially at light load and low speed. Figure 4 shows the comparison results of the cogging torque before and after the PMs of OPMSM offset.

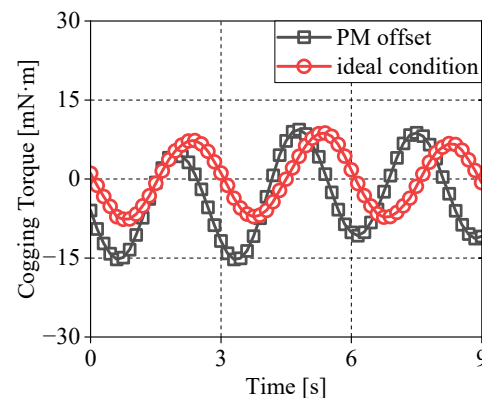


Figure 4. Cogging torque of PM offset and ideal condition.

It can be seen from Figure 4 that the phase of the cogging torque waveform changes after the PM offset, and the cogging torque amplitude increases compared with the ideal state. The analysis results show that the absolute value of the amplitude of the cogging torque after PM offset reaches 15.39 mN·m, while the absolute value of the amplitude in the ideal state is 8.82 mN·m, the amplitude of the cogging torque after PM offset is 74.49% higher than that in the ideal state, which makes the vibration and noise of the motor increase significantly during operation.

### 3.2. Air Gap Flux Density

Cogging torque is related to the air gap flux density on the armature surface, the expression of cogging torque can be expressed as follows:

$$T_{cog} = -\frac{\partial W}{\partial \theta} \quad (2)$$

where  $W$  is the magnetic field energy,  $\theta$  is the relative position between the stator and the rotor.

Ignoring the effect of core reluctance, the magnetic field energy storage in the motor can be expressed as the sum of the PM and the air gap magnetic energy:

$$W = W_{pm} + W_{gap} = \frac{1}{2\mu_0} \int_V B^2 dV \quad (3)$$

where  $B$  is the magnetic flux density,  $V$  is the air gap volume of the motor.

The air gap magnetic flux density distribution along the armature surface can be expressed as:

$$B(\theta, \alpha) = B_r(\theta)G(\theta, \alpha) \quad (4)$$

where  $B_r(\theta)$  is the remanent magnetic flux density of PM,  $\theta$  is the rotor position angle,  $G(\theta, \alpha)$  is the position function of the motor along the armature surface,  $\alpha$  is the angle between the stator tooth center line and the d-axis. The cogging torque can be expressed as:

$$T_{cog} = -\frac{\partial}{\partial \theta} \left[ \frac{1}{2\mu_0} \int_V B_r^2(\theta)G^2(\theta, \alpha) dV \right] \quad (5)$$

By expanding  $B_r(\theta)$  and  $G(\theta, \alpha)$  with Fourier series, respectively, the expression of cogging torque can be expressed as:

$$T_{cog} = \frac{\pi z L_a}{4\mu_0} (R_2^2 - R_1^2) \sum_{n=1}^{\infty} n G_n B_r\left(\frac{nz}{2p}\right) \sin(nz\alpha) \quad (6)$$

where  $z$  is the number of slots,  $p$  is the number of pole pairs,  $L_a$  is the length of the core,  $R_1$  and  $R_2$  has different meanings in different structure motors: in the inner rotor motor,  $R_1$  represents the outer diameter of the rotor and  $R_2$  represents the inner diameter of the stator; in the outer rotor motor,  $R_1$  represents the outer diameter of the stator and  $R_2$  represents the inner diameter of the rotor.

From the above formula, it can be concluded that the change in air gap flux density affects the cogging torque. Figure 5 shows the air gap flux density waveform and its harmonic in the offset state and ideal state of the PM.

It can be seen from Figure 5a that the upper half of the air gap flux density waveform is offset, which is consistent with the phenomenon of PM S-pole offset. The relative position offset of the air gap flux density is the direct cause of the increase in the cogging torque fluctuation and the change in the average cogging torque. Figure 5b shows that there is no significant difference in the fundamental amplitude of the air gap flux density before and after the PM offset, but the second, fourth, and sixth harmonics increase significantly after the PM offset. The increase in higher harmonics leads to the distortion of the air gap flux density waveform and increases the vibration and noise of the motor during operation.

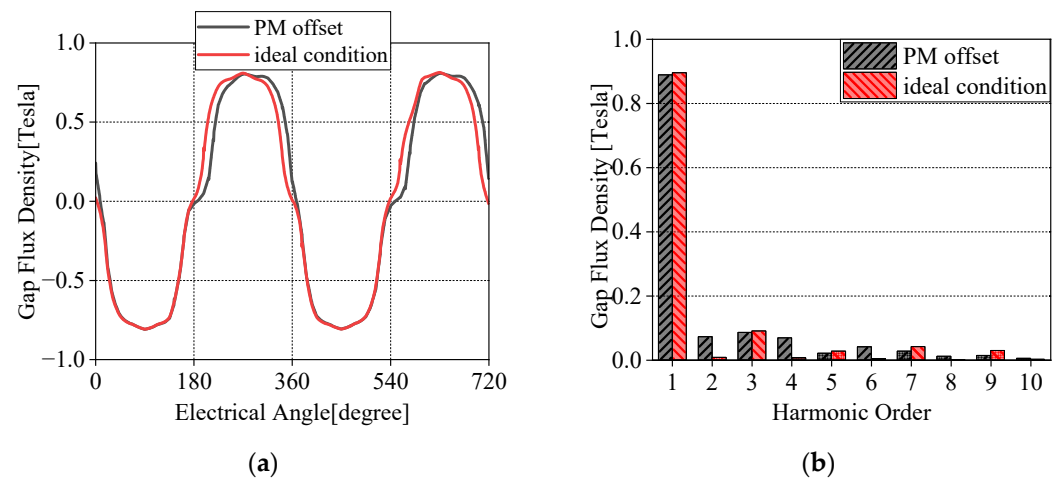


**Figure 5.** Air gap flux density of PM offset and ideal condition. (a) Waveforms; (b) harmonic spectra.

### 3.3. Electromagnetic Torque and Torque Ripple

Electromagnetic torque represents the output capacity of the motor. The torque ripple is composed of radial electromagnetic force, which is directly related to the noise and vibration level of the motor. Figure 6 shows the finite element analysis results of electromagnetic torque before and after PM offset.

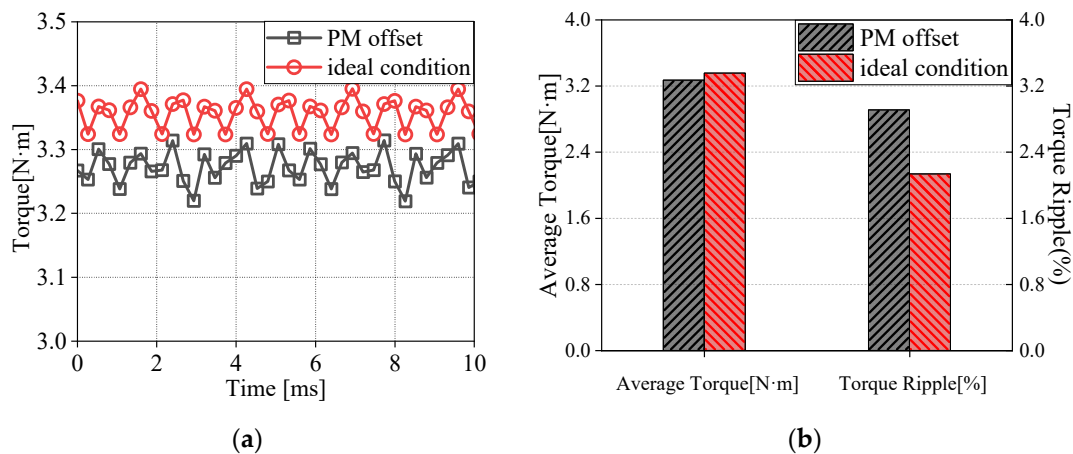


**Figure 6.** Torque of PM offset and ideal condition. (a) Waveforms; (b) average torque and torque ripple.

It can be seen from Figure 6 that the average torque in the ideal state of PM is higher than that in the state of PM offset. The average output torque is 3.36 N·m in ideal state and 3.27 N·m in the PM offset state, and the average output torque of the PM offset state is 2.68% lower than that of the ideal state. The torque ripple before and after PM offset is 2.14% and 2.91%, respectively, and the torque ripple of the PM offset state is 35.98% higher than that of the ideal state. It can be concluded that PM offset leads to a decrease in average torque and an increase in torque ripple, especially the torque ripple, which will lead to an increase in motor vibration and noise levels.

### 3.4. Back EMF

The back EMF waveform before and after the PM offset is shown in Figure 7. It can be seen from Figure 7 that when the PM is offset, the back EMF amplitude is 11.87 V and the effective value is 8.93 V. In the ideal state, the back EMF amplitude is 11.94 V. The effective value is 9 V. The back EMF amplitude of the PM offset state is 0.59% lower than that of the ideal state, and the back EMF effective value of the PM offset state is 0.78% lower than that of the ideal state. It can be concluded that the characteristics of back EMF before and after PM offset are similar.

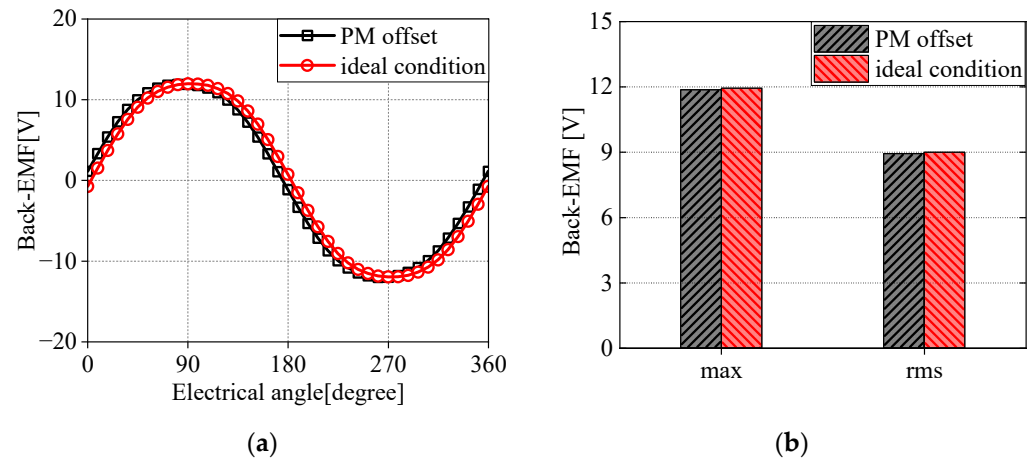


**Figure 7.** Back EMF of PM offset and ideal condition. (a) Waveforms; (b) max and rms.

#### 4. Analysis of Adding Auxiliary Teeth on the Surface of the Rotor Core

From the analysis results of the FEM in section III, it can be found that the PM offset has a negative impact on the electromagnetic characteristics of the OPMSM, especially the cogging torque, which changes greatly before and after the PM offset. Therefore, to ensure the high quality and performance unity of the motor production, it is necessary to eliminate the installation error of the PM in the large-scale production of the motor. By adding auxiliary teeth on the surface of the rotor core, the radial installation error of PM can be greatly reduced, as shown in Figure 8.

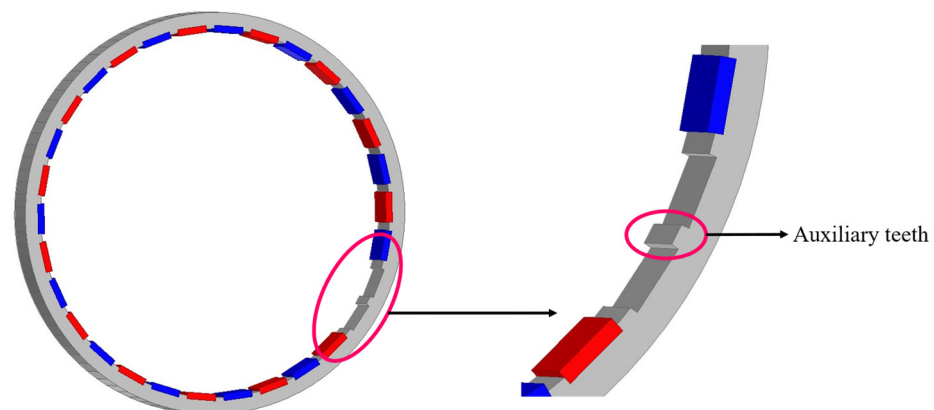


**Figure 8.** Rotor auxiliary teeth of OPMSM.

In this section, the parametric scanning method is used to analyze the influence of rotor auxiliary teeth on the electromagnetic characteristics of OPMSM. The influence of different teeth heights on the electromagnetic performance of the motor is analyzed, and the selection standard of the best auxiliary teeth height is determined so that the electromagnetic performance of OPMSM is affected by the rotor auxiliary teeth as small as possible. Then the OPMSM with different sizes and pole–slot ratios are compared and analyzed to verify the universality of the conclusion.

##### 4.1. Electromagnetic Characteristics

The air gap flux density is maintained at a constant value, and the auxiliary teeth height is linearly changed. The electromagnetic characteristics of OPMSM with different teeth heights are observed. Figure 9 shows the electromagnetic torque characteristics of the OPMSM under different rotor teeth heights, including electromagnetic torque waveform, average torque curve, and torque ripple curve.

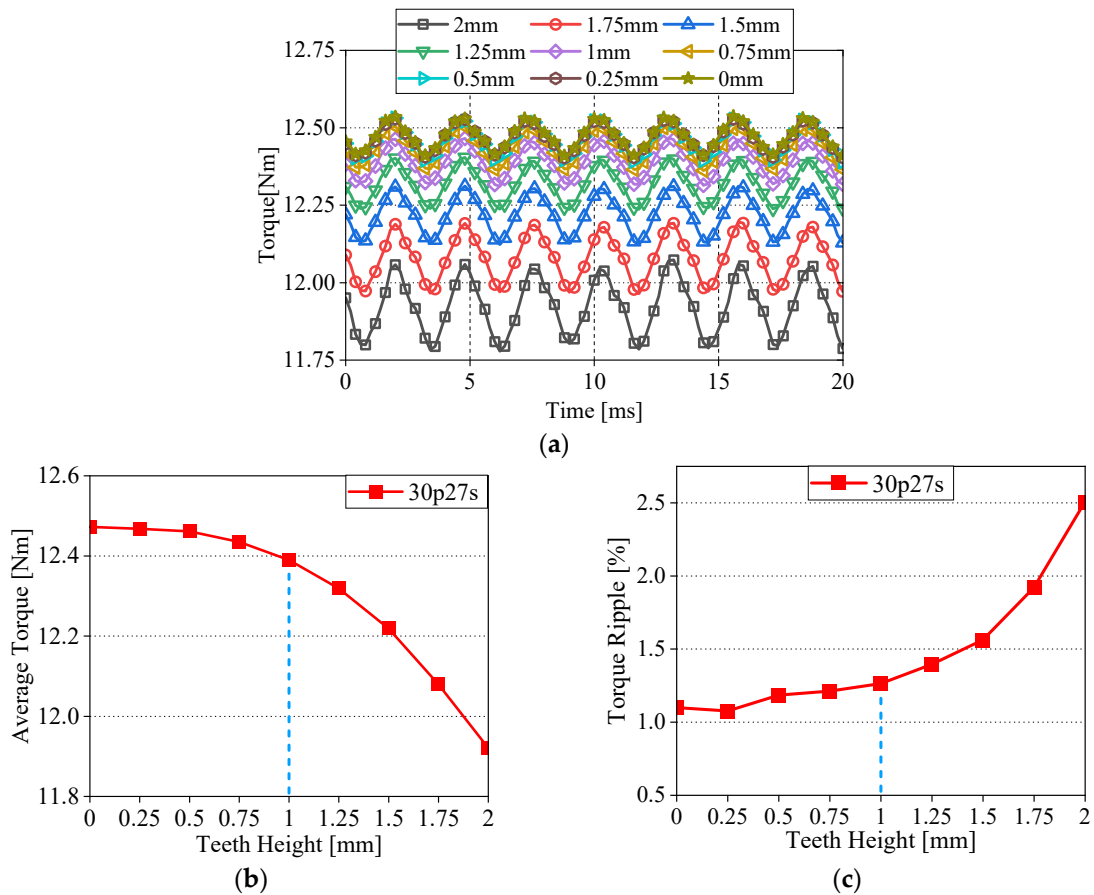


**Figure 9.** Electromagnetic torque characteristics of the OPMSM under different rotor teeth heights. (a) Electromagnetic torque waveform; (b) average torque curve; (c) torque ripple curve.

It can be seen from Figure 9 that the average electromagnetic torque decreases with the increase in the rotor teeth height, and the torque ripple increases with the increase in the teeth height. Figure 10 shows the air gap flux density waveform and its harmonic spectrum at different rotor teeth heights. Figure 11 shows the back EMF amplitude and its waveform distortion rate at different rotor teeth heights. It can be seen from Figure 10 that as the rotor teeth height increases, the sudden change trend of the air gap flux density waveform gradually increases near the q-axis (at  $0^\circ$ ,  $180^\circ$ , and  $360^\circ$  electrical angles in Figure 10). The Fourier expansion of the air gap flux density waveform is carried out to obtain the harmonic spectrum diagram of the air gap flux density in Figure 10b, it can be obtained that the fundamental amplitude decreases with the increase in the rotor teeth height, and the 5th and 7th harmonic amplitude increases with the increase in the rotor teeth height. Figure 11 shows that the back EMF amplitude increases with the increase in the rotor teeth height, but the harmonic distortion rate decreases with the increase in the rotor teeth height.

Summarizing the variation law of electromagnetic characteristics, it can be concluded that as the height of the rotor teeth changes linearly, the average torque, torque ripple, air gap flux density fundamental amplitude, back EMF amplitude, and back EMF harmonic distortion rate all change nonlinearly. The change trend is slow at the beginning, and the change speed increases significantly with the increase in rotor teeth height. In addition to the harmonic distortion rate, the electromagnetic characteristics are caused by the increase in the rotor teeth height, which leads to a decrease in the motor performance. However, when the rotor teeth height increases, the mechanical structure stability of OPMSM will be improved. Therefore, it is necessary to increase the height of the rotor teeth while ensuring that the electromagnetic performance does not change too much.



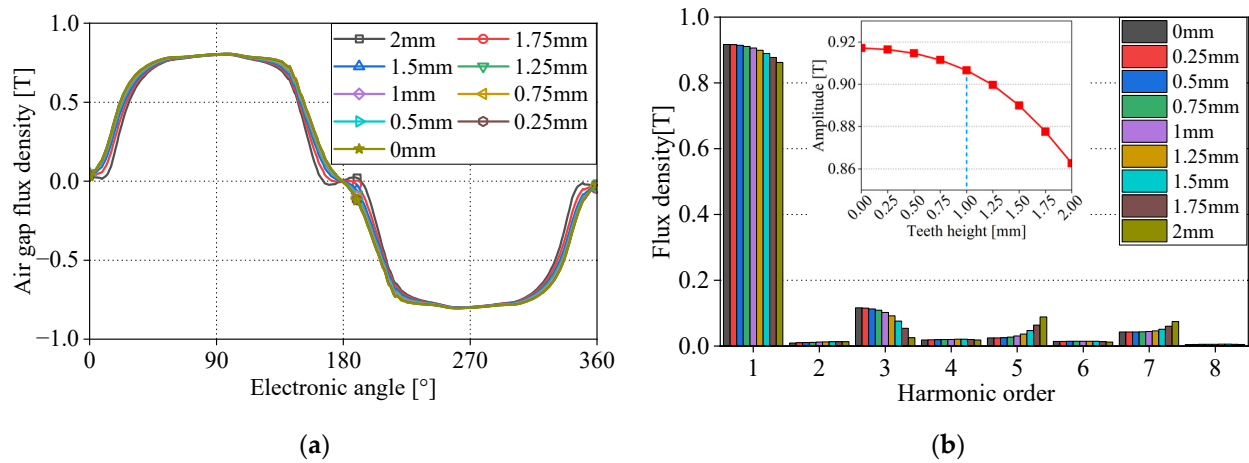


Figure 10. Air gap flux density under different rotor teeth heights. (a) Waveform; (b) harmonic spectrum.

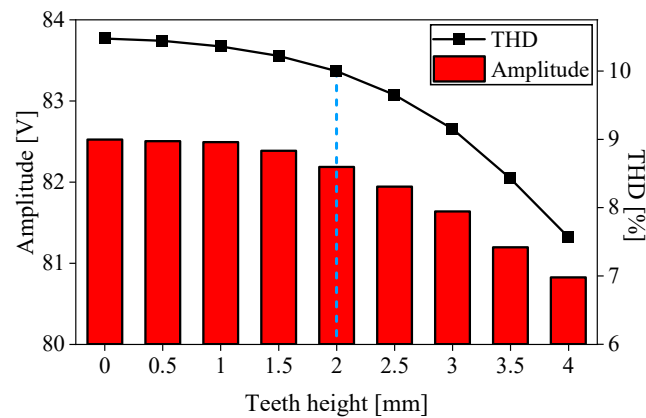


Figure 11. Back EMF amplitude and its waveform distortion rate under different rotor teeth heights.

By analyzing Figure 9b,c, Figures 10b and 11, it can be found that when the rotor teeth height is less than 1 mm (half of the radial thickness of PM), the electromagnetic performance changes little. When the rotor teeth height continues to increase, the electromagnetic performance changes significantly. Comparing the electromagnetic performance changes when the auxiliary teeth height increases from 0 to 1 mm and from 1 mm to 2 mm, the average torque decreases by 0.66% and 3.78%, respectively. The torque ripple increases by 14.94% and 98.43%, respectively. The air gap flux density fundamental amplitude is reduced by 1.15% and 4.85%, respectively. The back EMF amplitude decreases by 0.17% and 0.90%, respectively. The back EMF waveform distortion rate is reduced by 5.50% and 19.06%, respectively. Therefore, it can be concluded that when the rotor teeth height is half of the radial thickness of the PM, the rotor teeth have little effect on the overall electromagnetic performance of OPMSM.

#### 4.2. Loss and Efficiency

Figure 12 shows the eddy current loss of the magnetic steel under different rotor teeth heights during the steady-state operation of the motor. Figure 13 shows the core loss of the stator core and rotor core of the motor.

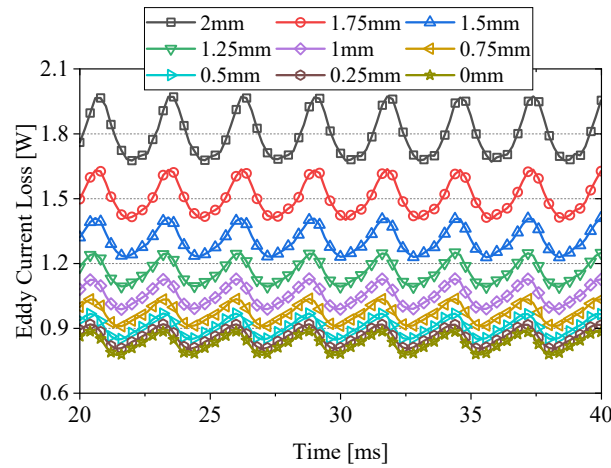


Figure 12. Eddy current loss of magnetic steel.

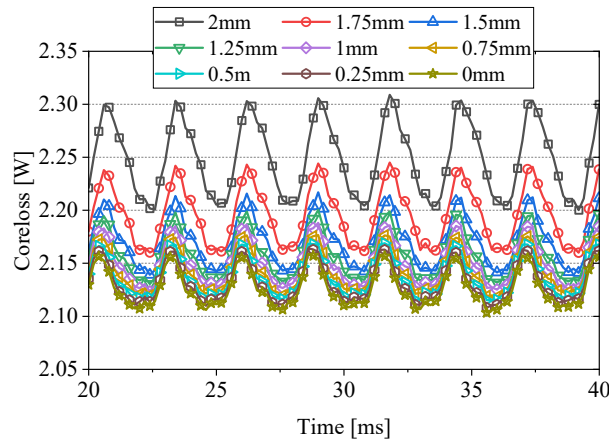


Figure 13. Core loss of the stator core and rotor core.

Copper loss can be calculated by formula (7).

$$P_{Cu} = mI^2R \tag{7}$$

where  $m$  is the number of phases,  $I$  is the effective value of the phase current, and  $R$  is the copper wire resistance.

$$R = \frac{1}{\sigma} \cdot \frac{L}{S} \tag{8}$$

where  $\sigma$  is the winding conductivity,  $L$  is the length of each phase winding wire, and  $S$  is the cross-sectional area of the wire.

Ignoring stray loss and mechanical loss, the efficiency of the motor is finally obtained. Figure 14 shows the efficiency of the motor at different rotor teeth heights.

It can be seen from Figure 14 that when the rotor teeth height increases from 0 to 1 mm, the efficiency is reduced by 0.14%. When the rotor teeth height increases from 1 mm to 2 mm, the efficiency is reduced by 0.68%. When the rotor teeth height increases from 0 to 1 mm, the efficiency of the motor decreases by nearly five times when the rotor teeth height increases from 0 to 1 mm. Therefore, it can be concluded that when the rotor teeth height is less than half of the radial thickness of the PM, the rotor teeth have little effect on the motor efficiency.

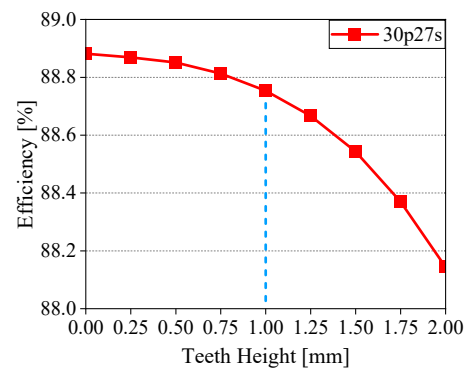


**Figure 14.** Efficiency under different rotor teeth heights.

#### 4.3. Universality Verification

To verify the universality of the above conclusions, the OPMSM with two different sizes and two different pole–slot ratios are compared and analyzed. The outer diameter of the original motor is 120 mm, the thickness of the PM is 2 mm, and the pole–slot ratio is 30p/27s. Table 2 is the data of motors for comparison.

**Table 2.** The parameters of OPMSMs for comparison.

Motor Type	Pole–Slot Ratio	Outer Diameter	Thickness of PM
Type 1	30p/27s	180 mm	3 mm
Type 2	30p/27s	240 mm	4 mm
Type 3	28p/24s	120 mm	2 mm
Type 4	16p/18s	120 mm	2 mm

Figure 15 is the torque waveform of motors for comparison. Figures 16 and 17 show the average torque and torque ripple curves, respectively. Figure 18 shows the air gap flux density waveform. Figure 19 shows the harmonic spectrum of the air gap flux density. Figure 20 shows the amplitude of the back EMF and its harmonic distortion rate. Figures 21 and 22 show the magnetic steel eddy current loss and the core loss, and Figure 23 shows the efficiency change in the motor. Table 3 summarizes the optimum auxiliary teeth height of four types of motors.

By analyzing the above figures, it can be concluded that when the size and pole–slot ratio of the OPMSM change, it does not affect the law that the electromagnetic characteristics change with the change in rotor teeth height. In addition to the change in the waveform distortion rate of the back EMF with the increase in the rotor teeth height, which will lead to the performance of the motor be better, the change in the average torque, torque ripple, air gap flux density, and the back EMF amplitude all lead to the decline of the motor performance, and the change speed of these electromagnetic characteristics is slow first and then fast. When the auxiliary teeth height is less than half of the radial thickness of the PM, adding auxiliary teeth has little effect on the overall performance of the motor.

It can be found that by adding rotor auxiliary teeth to the OPMSM and making its height about half of the radial thickness of the PM, the structural stability of the motor can be increased, the installation accuracy of PMs can be improved, and the influence of the installation error on the performance of OPMSM can be greatly reduced. At the same time, it has a small influence on the electromagnetic performance of the motor, making its electromagnetic performance close to the surface-mounted OPMSM and better than the surface-embedded OPMSM.

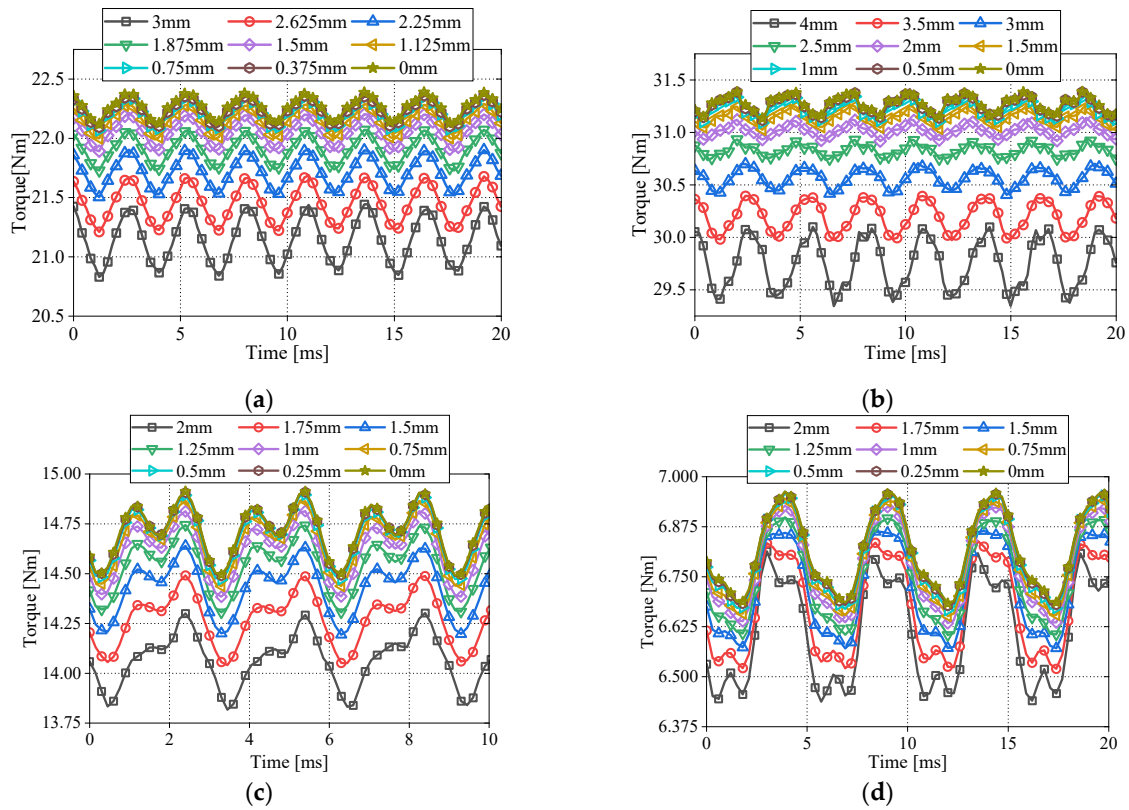


**Figure 15.** Electromagnetic torque waveforms under different rotor teeth heights. (a) Type 1; (b) Type 2; (c) Type 3; and (d) Type 4.

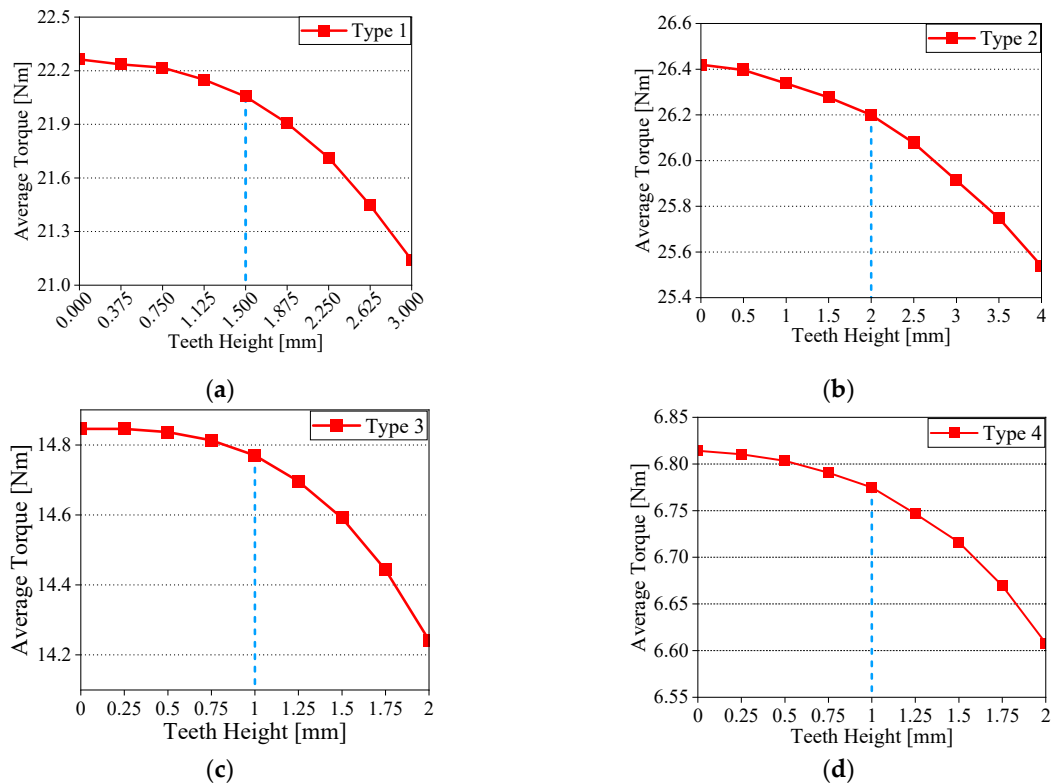


**Figure 16.** Average torque curve under different rotor teeth heights. (a) Type 1; (b) Type 2; (c) Type 3; and (d) Type 4.

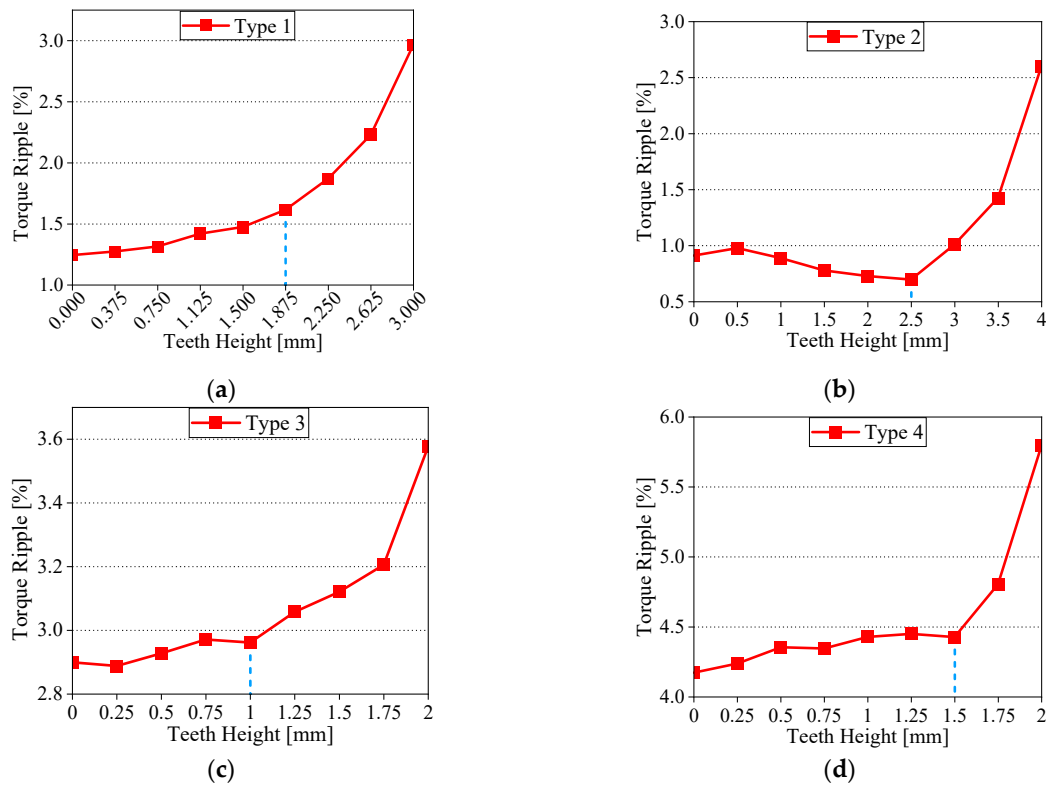


Figure 17. Torque ripple curve under different rotor teeth heights. (a) Type 1; (b) Type 2; (c) Type 3; and (d) Type 4.

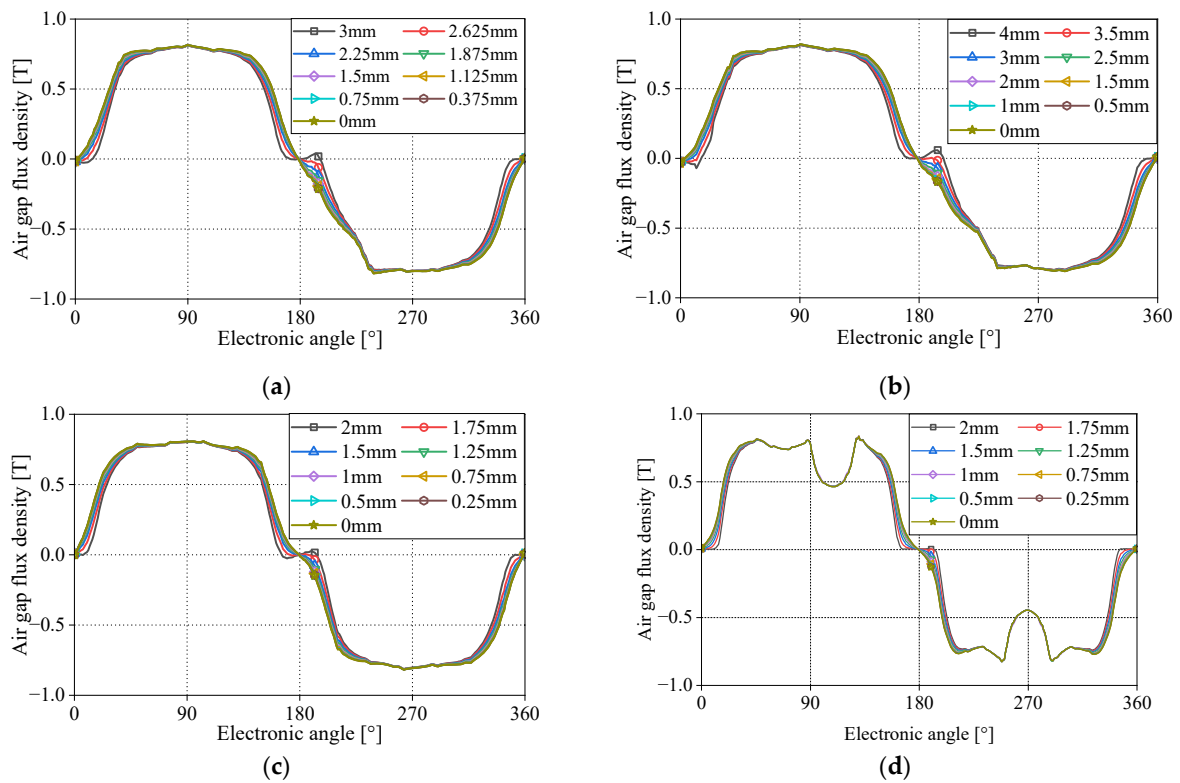


Figure 18. Air gap flux density waveforms under different rotor teeth heights. (a) Type 1; (b) Type 2; (c) Type 3; and (d) Type 4.

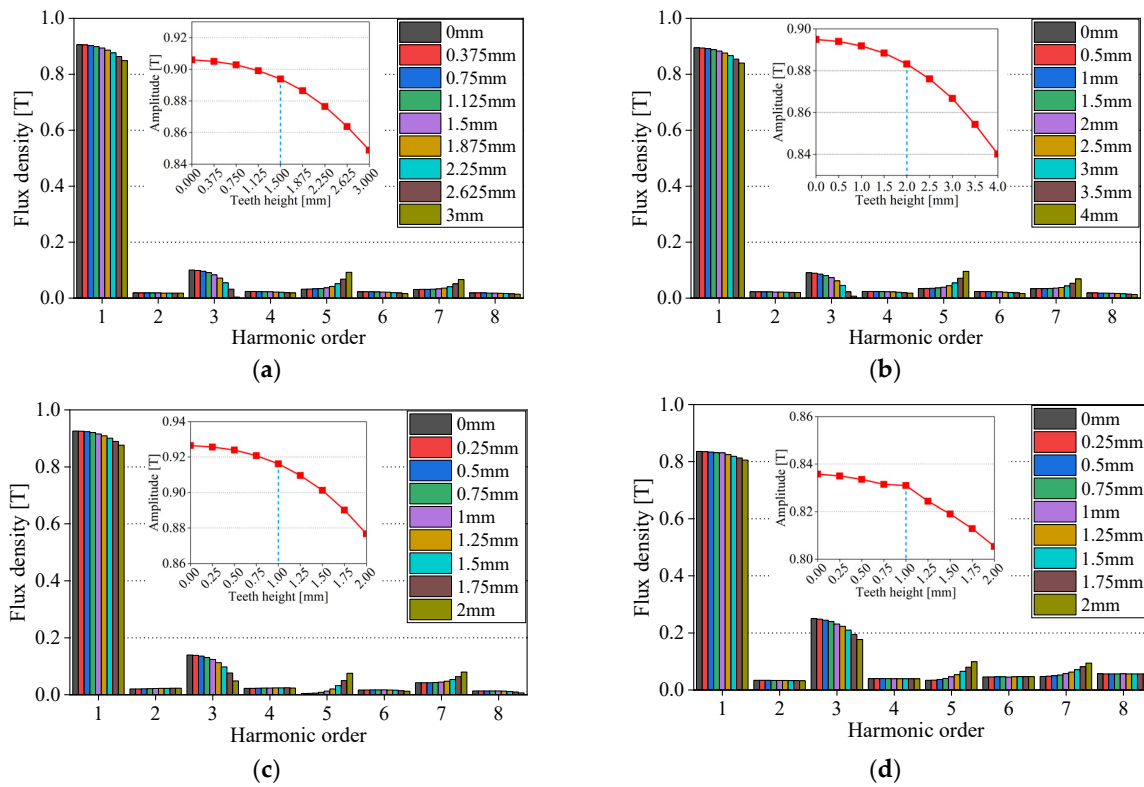


Figure 19. Air gap flux density harmonic spectrum under different rotor teeth heights. (a) Type 1; (b) Type 2; (c) Type 3; and (d) Type 4.

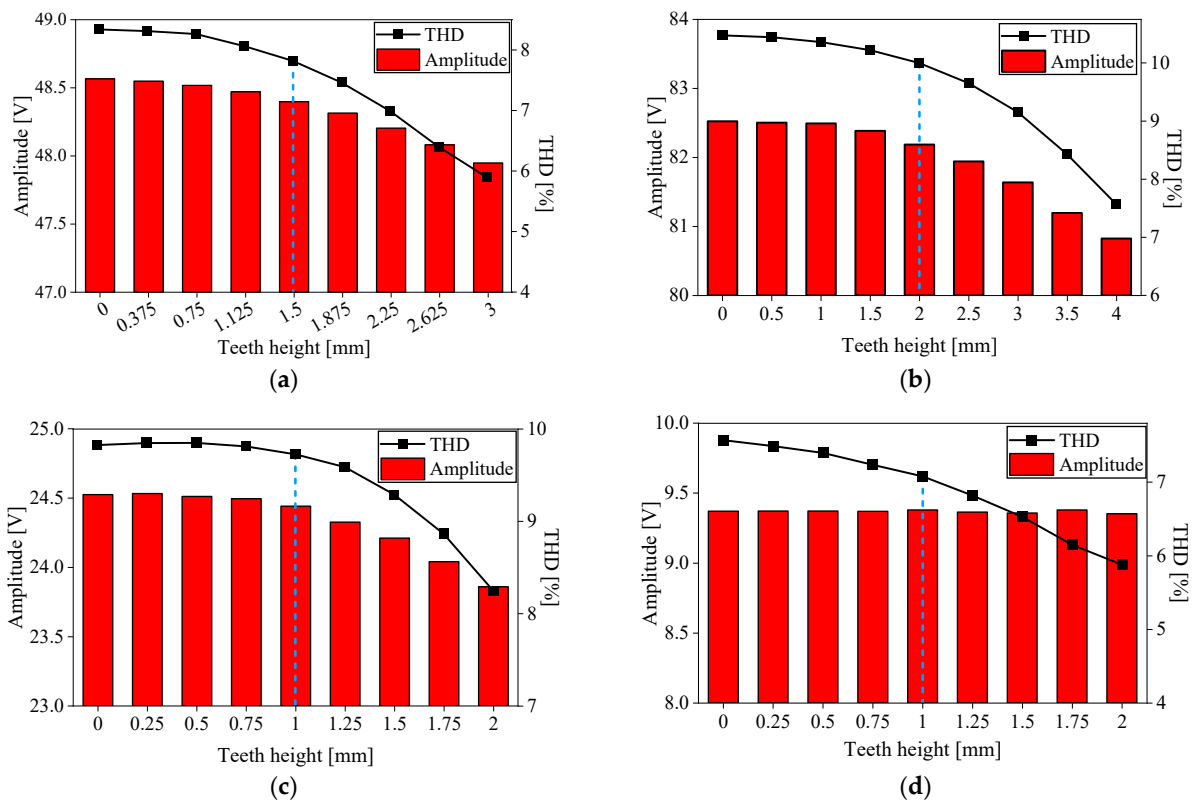
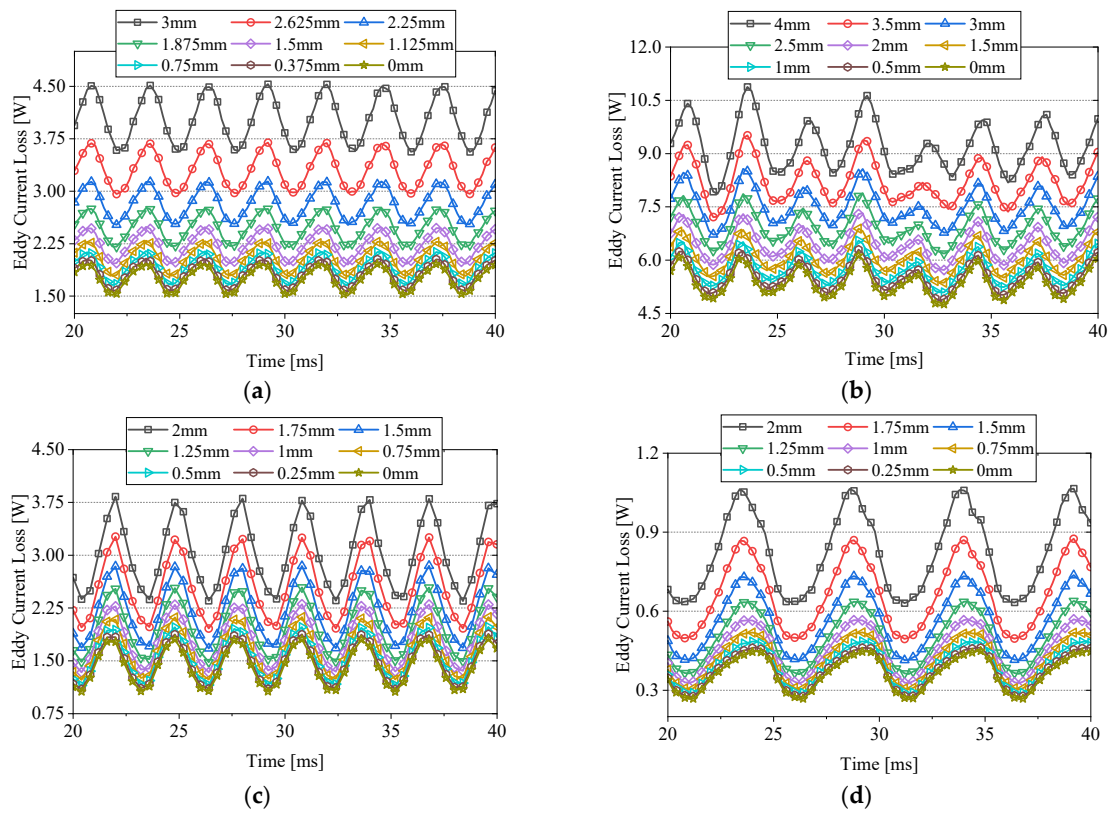
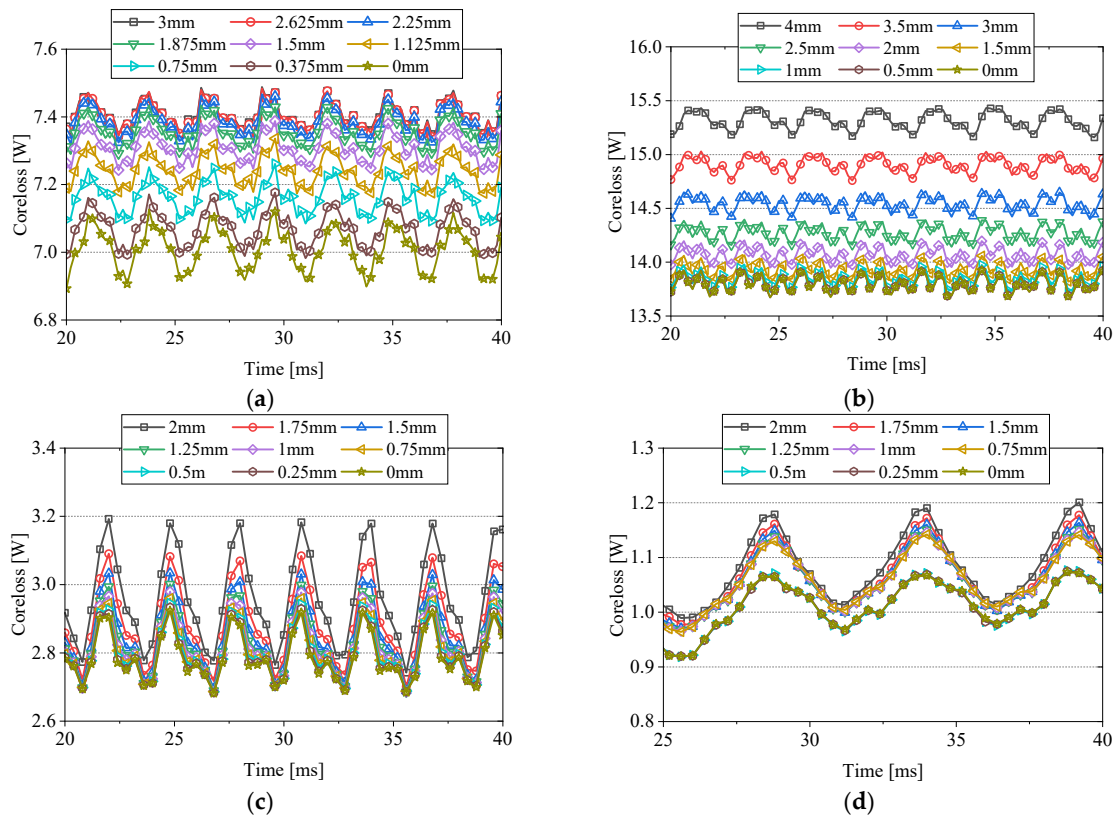


Figure 20. Back EMF amplitude and their waveform distortion rate under different rotor teeth heights. (a) Type 1; (b) Type 2; (c) Type 3; and (d) Type 4.



**Figure 21.** Eddy current loss of magnetic steel under different rotor teeth heights. (a) Type 1; (b) Type 2; (c) Type 3; and (d) Type 4.



**Figure 22.** Core loss of the stator core and rotor core under different rotor teeth heights. (a) Type 1; (b) Type 2; (c) Type 3; and (d) Type 4.

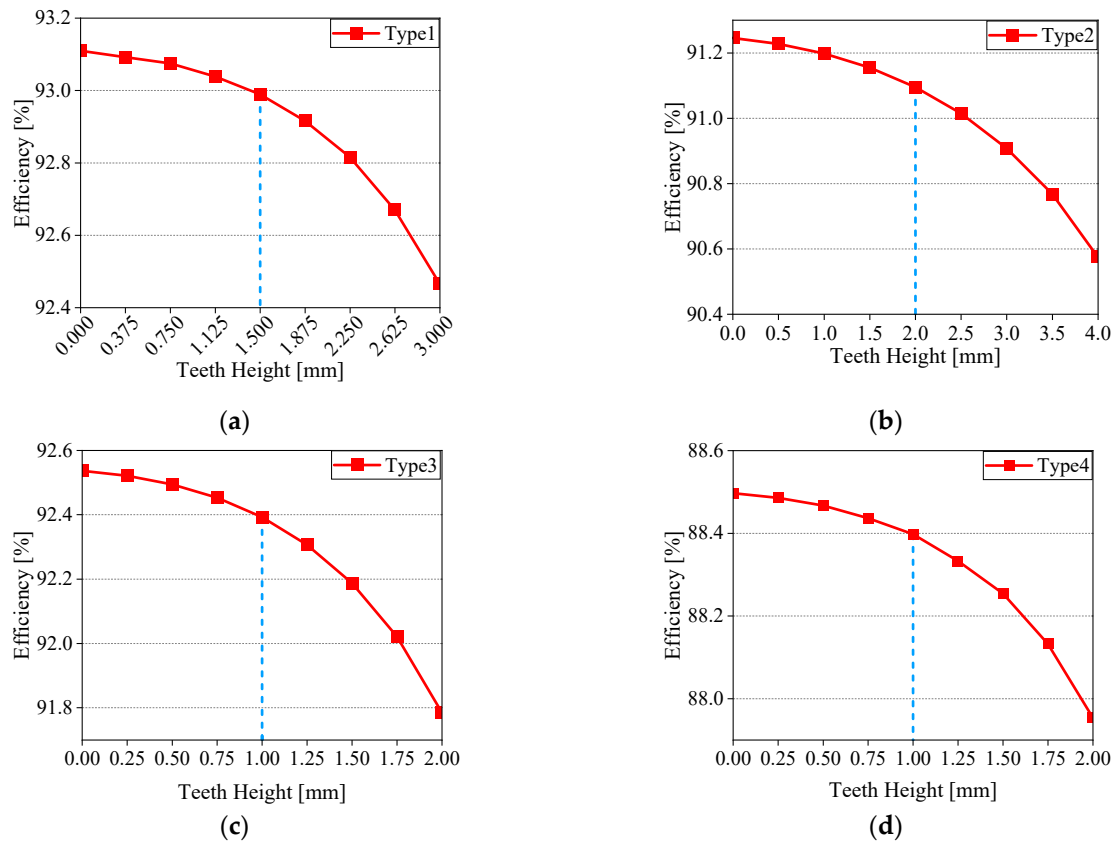


**Figure 23.** Efficiency under different rotor teeth heights. (a) Type 1; (b) Type 2; (c) Type 3; and (d) Type 4.

**Table 3.** The optimal auxiliary teeth height for the four types of motors.

Motor Type	Thickness of PM	The Optimal Auxiliary Teeth Height
Type 1	3 mm	1.5 mm
Type 2	4 mm	2 mm
Type 3	2 mm	1 mm
Type 4	2 mm	1 mm

## 5. Conclusions

The structural characteristics of the surface-mounted OPMSM lead to some inevitable errors in the installation of the PM of the motor, and these errors will have an influence on the electromagnetic characteristics of the motor. The optimization method of adding auxiliary teeth on the surface of the rotor core is studied in this paper, and the selection criteria of the optimal auxiliary teeth height is finally determined. Some conclusions are summarized as follows:

(1) The PM installation error of OPMSM has little effect on the back EMF of the motor but has a great influence on the cogging torque and torque ripple: the 1-degree offset of S-poles will lead to an increase of 74.49% in the cogging torque amplitude and an increase of 35.98% in the torque ripple, which will lead to increases in the vibration and noise. Such errors can be almost eliminated completely by adding auxiliary teeth on the surface of the rotor core. For large-scale motor assembly production, these factors must be considered to improve the quality and life of the product.

(2) Through the parametric model simulation analysis, it can be found that the process of some electromagnetic parameters changing with the change in auxiliary teeth height is nonlinear, so the most suitable auxiliary teeth height can be found by parametric scanning method, which can reduce the PM installation error and enhance the structural stability



of OPMSM while ensuring that the electromagnetic characteristics of the motor are not greatly affected. The analysis result shows that the optimal auxiliary teeth height of OPMSM is about half of the radial thickness of the PM, which can make the electromagnetic characteristics of OPMSM close to surface-mounted OPMSM and better than surface-embedded OPMSM. The wide applicability of this conclusion is verified by comparing and analyzing OPMSM with different sizes and different pole–slot ratios.

**Author Contributions:** Conceptualization, J.S. (Jiayin Su) and R.N.; methodology, J.S. (Jiayin Su) and R.N.; software, J.S. (Jiayin Su); validation, J.S. (Jiayin Su); formal analysis, J.S. (Jiayin Su) and P.W.; investigation, J.S. (Jiayin Su); resources, R.N., P.W. and J.S. (Jikai Si); data curation, J.S. (Jiayin Su); writing—original draft preparation, J.S. (Jiayin Su); writing—review and editing, J.S. (Jiayin Su) and R.N.; visualization, J.S. (Jiayin Su); supervision, S.X., J.L. and J.S. (Jikai Si). All authors have read and agreed to the published version of the manuscript.

**Funding:** This work was supported by the National Natural Science Foundation of China (52207067, 52277069, 52307070), the Henan Province Science and Technology Research and Development Plan Joint Fund (Application Research) (232103810088), the China Postdoctoral Science Foundation (2023M743155), the Henan Province Key R&D and promotion projects (Scientific and Technological Breakthrough) (232102221016), and the Major Special Project for Collaborative Innovation in Zhengzhou (20XTZX12023).

**Data Availability Statement:** The original contributions presented in the study are included in the article, further inquiries can be directed to the corresponding author/s.

**Conflicts of Interest:** The authors declare no conflict of interest.

## References

1. Wu, L.J.; Zhu, Z.Q.; Staton, D.A.; Popescu, M.; Hawkins, D. Comparison of Analytical Models of Cogging Torque in Surface-Mounted PM Machines. *IEEE Trans. Ind. Electron.* **2012**, *59*, 2414–2425. [[CrossRef](#)]
2. Zhou, X.; Zhu, X.; Wu, W.; Xiang, Z.; Liu, Y.; Quan, L. Multi-objective Optimization Design of Variable-Saliency-Ratio PM Motor Considering Driving Cycles. *IEEE Trans. Ind. Electron.* **2021**, *68*, 6516–6526. [[CrossRef](#)]
3. Zhou, Y.; Li, H.; Meng, G.; Zhou, S.; Cao, Q. Analytical Calculation of Magnetic Field and Cogging Torque in Surface-Mounted Permanent Magnet Machines Accounting for Any Eccentric Rotor Shape. *IEEE Trans. Ind. Electron.* **2015**, *62*, 3438–3447. [[CrossRef](#)]
4. Kefalas, T.D.; Kladas, A.G. Thermal Investigation of Permanent-Magnet Synchronous Motor for Aerospace Applications. *IEEE Trans. Ind. Electron.* **2014**, *61*, 4404–4411. [[CrossRef](#)]
5. Yu, Y.; Pei, Y.; Chai, F.; Doppelbauer, M. Performance Comparison Between Permanent Magnet Synchronous Motor and Vernier Motor for In-Wheel Direct Drive. *IEEE Trans. Ind. Electron.* **2023**, *70*, 7761–7772. [[CrossRef](#)]
6. Zhang, W.; Xu, Y.; Zhou, G. Research on a Novel Transverse Flux Permanent Magnet Motor with Hybrid Stator Core and Disk-Type Rotor for Industrial Robot Applications. *IEEE Trans. Ind. Electron.* **2021**, *68*, 11223–11233. [[CrossRef](#)]
7. Zuo, S.; Lin, F.; Wu, X. Noise Analysis, Calculation, and Reduction of External Rotor Permanent-Magnet Synchronous Motor. *IEEE Trans. Ind. Electron.* **2015**, *62*, 6204–6212. [[CrossRef](#)]
8. Wu, Z.Z.; Zhu, Z.Q.; Zhan, H.L. Comparative Analysis of Partitioned Stator Flux Reversal PM Machines Having Fractional-Slot Nonoverlapping and Integer-Slot Overlapping Windings. *IEEE Trans. Energy Convers.* **2016**, *31*, 776–788. [[CrossRef](#)]
9. Magnussen, F.; Lendenmann, H. Parasitic Effects in PM Machines with Concentrated Windings. *IEEE Trans. Ind. Appl.* **2007**, *43*, 1223–1232. [[CrossRef](#)]
10. El-Refaie, A.M. Fractional-Slot Concentrated-Windings Synchronous Permanent Magnet Machines: Opportunities and Challenges. *IEEE Trans. Ind. Electron.* **2010**, *57*, 107–121. [[CrossRef](#)]
11. Cao, Z.; Liu, J. Cogging Torque Reduction for Outer Rotor Interior Permanent Magnet Synchronous Motor. In Proceedings of the IECON 2020—46th Annual Conference of the IEEE Industrial Electronics Society, Singapore, 18–21 October 2020; pp. 2689–2693. [[CrossRef](#)]
12. Ou, J.; Liu, Y.; Qu, R.; Doppelbauer, M. Experimental and Theoretical Research on Cogging Torque of PM Synchronous Motors Considering Manufacturing Tolerances. *IEEE Trans. Ind. Electron.* **2018**, *65*, 3772–3783. [[CrossRef](#)]
13. Nakano, M.; Morita, Y.; Matsunaga, T. Reduction of Cogging Torque Due to Production Tolerances of Rotor by Using Dummy Slots Placed Partially in Axial Direction. *IEEE Trans. Ind. Appl.* **2015**, *51*, 4372–4382. [[CrossRef](#)]
14. Simon-Sempere, V.; Burgos-Payan, M.; Cerquides-Bueno, J.-R. Influence of Manufacturing Tolerances on the Electromotive Force in Permanent-Magnet Motors. *IEEE Trans. Magn.* **2013**, *49*, 5522–5532. [[CrossRef](#)]
15. Gerling, D. Analytical calculation of the PM machine magnetic field depending on magnet width and skewing. In Proceedings of the 2009 13th European Conference on Power Electronics and Applications, Barcelona, Spain, 8–10 September 2009; pp. 1–7.
16. Gasparin, L.; Cernigoj, A.; Markic, S.; Fiser, R. Additional Cogging Torque Components in Permanent-Magnet Motors Due to Manufacturing Imperfections. *IEEE Trans. Magn.* **2009**, *45*, 1210–1213. [[CrossRef](#)]

17. Wu, W.-H.; Zhu, Y.-D.; Yu, D.-G. Parametric analysis of the magnet location based on straight-shape internal permanent magnet synchronous motor. In Proceedings of the 2017 IEEE International Conference on Cybernetics and Intelligent Systems (CIS) and IEEE Conference on Robotics, Automation and Mechatronics (RAM), Ningbo, China, 19–21 November 2017; pp. 316–321. [[CrossRef](#)]
18. Heins, G.; Brown, T.; Thiele, M. Statistical Analysis of the Effect of Magnet Placement on Cogging Torque in Fractional Pitch Permanent Magnet Motors. *IEEE Trans. Magn.* **2011**, *47*, 2142–2148. [[CrossRef](#)]

**Disclaimer/Publisher’s Note:** The statements, opinions and data contained in all publications are solely those of the individual author(s) and contributor(s) and not of MDPI and/or the editor(s). MDPI and/or the editor(s) disclaim responsibility for any injury to people or property resulting from any ideas, methods, instructions or products referred to in the content.